SUPPLEMENTAL MATERIAL

Supplementary methods

Mice

FGF21 knockout mice in C57BL/6J background were generated as previously described[1]. C57BL/6J apoE$^{-/-}$ mice were obtained from Jackson Laboratory. ApoE$^{-/-}$ mice were backcrossed with FGF21$^{-/-}$ mice for at least ten generations to obtain apoE$^{-/-}$ / FGF21$^{-/-}$ mice (namely DKO mice). β-klotho-floxed mice were generated by Shanghai Nanfang Center for Model Organisms, and were used to produce β-klotho liver specific knockout mice (β-klotho LKO) by injecting with adeno-associated virus encoding Cre recombinase (AAV-Cre) under the control of the mouse *apoE* gene promoter. All the mice were housed in a room at controlled temperature [23±1°C] with a 12 hour light-dark cycle, and had free access to water and standard rodent diet. For the intervention studies, 8-week-old DKO and β-klotho LKO mice were treated with recombinant full-length adiponectin produced from mammalian cells[2] and recombinant mouse FGF21[3] by daily intraperitoneal injection respectively. Glucose and insulin tolerance tests were performed as described previously[4]. All the animal studies were approved by the animal research ethics committee of Wenzhou Medical University and the University of Hong Kong.

Analysis of Atherosclerotic Lesions

Oil red O staining was used to assess the size of the atherosclerotic lesion as previously described[5, 6] with slight modifications. For *en face* analyses of lesions in the entire aorta, after perfusion，whole aorta was dissected out, opened longitudinally from heart to the iliac arteries, pinned on a black wax pan, and stained with Oil red O. The images of the aorta were captured using a SONY DXC-970MD color video camera, analyzed with the Image-Pro plus program

(Media Cybernetics, Silver Spring, MD), and presented as the percentage of lesion area in whole aorta.

For analysis of plaque lesion in aortic sinus, the heart and proximal aorta were removed and embedded in optimum cutting temperature compound. Serial 10μm-thick cryosections from the middle portion of the ventricle to the aortic arch were collected. For analysis of lesion in brachiocephalic arteries, serial 10μm-thick cryosections from a 150μm-distance position to aortic arch were collected. Then, cryosections of aortic sinus and brachiocephalic arteries were stained with Oil Red O and hematoxylin. The lipid-containing area on each section was determined in a blinded fashion, using an ocular piece with a 20×20 μm^2 grid on a light microscope. The average lesion area per aorta, calculated from 5 to 10 sections of each aorta, was determined.

Immunocytochemistry

The cryosections of mouse aortic arches were fixed in acetone and blocked with non-immune rabbit serum, followed by incubation with a rabbit polyclonal antibody against the macrophage marker F4/80 (Abcam, Cambridge, MA) or smooth muscle α-actin (Sigma, St Louis, MO) for 90 minutes. After washing, the sections were incubated with a FITC- or Cy3-labeled secondary goat anti-rabbit antibody for 30min. All the slides were examined under the Olympus biological microscope BX41, and the images were recaptured with an Olympus DP72 color digital camera. Planimetry on the photographed cross-sections was performed using Image-Pro Plus version 5.0.1 (Media Cybernetics, Inc, Bethesda, MD). The lesion areas were defined as an area between the lumen and internal elastic lamina, and the cell contents were presented as the percentage of positive surface areas in the lesion area.

Measurement of Cholesterol/cholesteryl Ester Levels in the Brachiocephalic arteries

The analysis of cholesterol/cholesteryl ester abundance was measured with a commercial kit according to the manufacturer instruction (abcam 65359, Abcam, Cambridge, UK). Briefly, the brachiocephalic artery was dissected free of adventitial tissue, weighed, extracted with 200μl of chloroform: Isopropanol: NP-40 (7:11:0.1) in a micro-homogenizer after weighting, and centrifuged at 15,000 x g for 10 minutes. The organic phase was transferred to a new

tube and air-dried at 50°C followed by vacuum drying for 30 min to remove trace organic solvent. The lipids were then dissolved with 200μl of Cholesterol Assay Buffer. 50ul of the samples or standard cholesterol were incubated with the reaction mixture including cholesterol esterase, cholesterol enzyme mix and cholesterol probe for 60 minutes at 37°C, followed by measurement of absorbance at 570nm with a microplate reader. Data were expressed as μmole cholesterol/cholesteryl ester per g tissue.

Biochemical and Immunological Assays

Plasma lipid profiles including total triglycerides, total-, HDL- and LDL-cholesterol levels were measured with commercial kits from Sigma, (St. Louis, MO). Liver total lipids were extracted with acetone and chloroform/methanol (2/1, v/v) as described[7], and total cholesterol levels in the liver were quantified as above and expressed as mg cholesterol per gram liver tissue (wet). Plasma levels of insulin and total adiponectin were measured using immunoassays from Antibody and Immunoassay Services at the University of Hong Kong. MCP-1 and TNF-α concentrations were analyzed with immunoassays from R&D System Inc (Minneapolis, MN).

Measurement of Cholesterol Absorption

Intestinal cholesterol absorption was determined by a fecal dual-isotope ratio method[8]. Briefly, mice were injected with 2.5 μCi ^{3}H-cholesterol in Intralipid (Sigma, St Louis, MO, USA) via tail vein, followed by oral gavage of 1 μCi ^{14}C-cholesterol in median-chain triglycerides (MCT oil, Mead Johnson, Evansville, IN). Mice were returned to cage with free access to food and water. After 72 h, blood samples were collected and the radioactivity of ^{14}C and ^{3}H were determined by scintillation counting. Intestine cholesterol absorption was determined as the ratio of ^{14}C/^{3}H in 1 ml of plasma.

Hepatic *de novo* Cholesterol synthesis

Hepatic cholesterol synthesis was determined as previous described[9]. Mice fasted for 4 hours were intraperitoneally injected with 10 μCi of [1-^{14}C]-sodium acetate (Perkin Elmer, Waltham, MA), and were then sacrificed at 30min after injection to harvest liver tissue. Approximately 250mg of liver tissue was rinsed in ice-cold PBS, and then saponified in 2.2

ml mixture of 50% KOH: 95% ETOH (1:10, v: v) at 70°C overnight. ^{3}H-cholesterol (1 μCi) was added to the same tube as a recovery control. Sterols were extracted with 3 ml hexane, dried and redissolved in 300μl mixture of acetone : ETOH (1:1, v: v), followed by precipitation with 1 ml of digitonin (0.5% in 95% ETOH) overnight at room temperature. The radioactivity of ^{3}H and ^{14}C in the precipitates was determined in a scintillation counter. Cholesterol synthesis rate was expressed as the amount of [1-^{14}C]-acetate incorporated into sterols per minute per gram liver tissue.

Measurement of Fecal Cholesterol and Bile Acids

Feces were collected from individually housed mice over a 3-day period and were dried, weighed, and ground to a powder. Lipids were extracted from feces with chloroform /methanol (2:1), dried, and dissolved with 5% Triton X-100 in isopropanol. Cholesterol contents were quantified using a biochemical assay. For analysis of bile acids, 50 mg of dried feces were added to 2.2 ml ethanolic NaOH (0.08M) and heated (95°C) for 2 h. After cooling, neutral sterols were extracted three times with 5 ml hexane, followed by acidification with 2.5 ml of 0.16M HCI and extraction with 5 ml of ethyl acetate. The dried extract was solubilized in 1.25% Triton X-100 in 20% methanol. Bile acids in each sample were determined with a Bile Acid Assay Kit (Genzyme Diagnostic, Framingham, MA).

RNA Extraction and Real-Time PCR

Total RNA was extracted from liver or adipose tissues with TRIzol reagent (Invitrogen), and complementary DNA was synthesized from 0.5μg total RNA by reverse transcription with an ImProm-II reverse transcription kit (Promega) with random hexamer primers. Quantitative real-time PCR was performed on the Applied Biosystems Prism 7000 sequence detection system, with specific primers described in Supplementary Table 1. The amplification efficiency, as calculated from the slope of each standard curve using the formula $E=10^{[-1/Slope]}\times100$, is between 92 and 105%. The relative expression level of each gene was calculated with the Pfaffl methods as previously described[10], using the β-actin gene as the reference control for normalization.

Srebp-1 and Srebp-2 DNA Binding Activity Assay

Srebp-1 and -2 DNA binding activities were measured by a commercial kit according to the manufacturer instruction (ab133125 and ab133111, Abcam Cambridge, UK). In brief, approximately 10mg nuclear extracts isolated from liver tissue were added to 96-well microplates coated with a specific double strand DNA (dsDNA) sequence containing with Srebp-1 or -2. The unbound reagents were removed by extensive washing, followed by sequential incubation with a primary antibody against Srebp-1 or -2 for 2 h, and a HRP-conjugated secondary antibody was added and incubated for 30 minutes. After washing, the substrate reagents were added, and the absorbance values at 450nm were measured with a microplate reader.

Construction of Adenoviral Vectors for Knockdown Srebp-2, FGFR2, FGFR3 and FGFR4 or Overexpression of Srebp-2

An adenovirus delivery system was used for knocking down Srebp-2, FGFR2, FGFR3 and FGFR4 expression with small hairpin RNA as well as for overexpression of Srebp-2. The oligonucleotides for generation of siRNA against these genes as well as the corresponding scrambled controls are listed in Supplementary Table 2. The forward and reverse oligonucleotides were annealed, ligated into pENTR/U6 entry vector, and then subcloned into pAd/BLOCK-iT DEST vector through recombination. To construct adenoviral vectors for overexpression of Srebp-2, cDNA encoding amino acids 1–460 of mouse Srebp-2 was inserted into pshuttle-CMV vector, and then subcloned into pAdeasy-1 adenoviral backbone vector (Stratagene) through recombination in Escherichia coli.

To package adenovirus, the adenoviral vectors were linearized with the restriction enzyme PacI and transfected into HEK293 cells using Lipofectamine 2000. After several rounds of propagation, recombinant adenovirus was purified by an AdEasy virus purification kit (Stratagene), and the titer was determined with an endpoint assay as described[11].

Smooth Muscle Proliferation and Migration Assays

Human aortic smooth muscle cells (HASMCs) were maintained in a humidified 37 °C and 5% CO_2 environment in OPTI-MEM® supplemented with 10% fetal bovine serum, 0.01 mg/ml

insulin, 0.01 mg/ml transferrin, 10 ng/ml sodium selenite, 0.03 mg/ml endothelial cell growth supplement, and 0.05 mg/ml ascorbic acid. Cells were routinely split at a 1:4 ratio, and cultures between the third to eighth passages were used. For proliferation analysis, cells were plated in 24-well plates (8000 and 10000 cells/well for HASMCs) and grown for 24 h. Medium was then replaced with DMEM with 0.1% BSA for 24 h. The medium was subsequently changed to fresh DMEM with 1% fetal bovine serum plus PDGF-BB (10ng/ml), recombinant mouse FGF21 (50ng/ml) and/or recombinant mouse adiponectin (2.0μg/ml). 18 h after incubation, 1 μCi of [*methyl*-^{3}H] thymidine was added into each well for another 6 h, and the amount of [^{3}H] thymidine incorporated into DNA in each well was determined as we described previously[12].

To assess cell migration, a Boyden chamber assay was performed using Transwell chambers (6.5mm, model 3422; Costar, Cambridge, MA, USA) with an 8-mm pore polycarbonate membrane[13]. Growth-arrested HASMC were harvested, suspended in serum-free DMEM. Cells were added to the upper chamber of the Transwell at 5×10^5 cells in 100 μl/well. A total of 600 μl of serum-free DMEM was added to the lower chamber, followed by treatment with PDGF-BB(10ng/ml), recombinant full-length adiponectin (2.0μg/ml) or recombinant mouse FGF21(50ng/ml) for 24 h respectively. Afterwards, the nonmigratory cells were removed from the upper surface of the membrane by scraping with cotton swabs. Membrane was then fixed with methanol, stained with Diff-Quik solution (Baxter, McGaw Park, IL, USA) and mounted on a glass slide. Migrated cells were counted at x400 magnification in 10 microscope fields per filter.

Analysis of Macrophage Uptake of Acetylated LDL (AcLDL)

AcLDL labeled with the fluorescent probe 3,3,39,39-tetramethylindocarbocyanine perchlorate（Dil-AcLDL）and unlabeled AcLDL were purchased from Biomedical Technologies (Ward Hill, MA 01835 USA). Primary mouse peritonealmacrophages grown in a serum-free RPMI-1640 medium were treated with mouse adiponectin (2.0μg/ml) or rmFGF21(50ng/ml) for 24 h, and were then incubated with 10μg/ml Dil-AcLDL dissolved in RPMI-1640 containing 2% lipoprotein-deficient serum (Sigma, St. Louis, Missouri, USA) for 3 hours. For competition assays, unlabeled AcLDL in excess amounts (50-fold) were added

together with Dil-AcLDL. The cells were resuspended in PBS and analyzed using a FACScan flow cytometer (Becton Dickinson). Specific fluorescent intensity was calculated by subtracting autofluorescent intensity from the mean fluorescent intensity of DiI-labeled cells. The uptake of Dil-AcLDL was calculated by subtracting binding in presence of excess amount of unlabeled AcLDL from total binding in absence of unlabeled acLDL, and expressed as fold changes over untreated cells.

Generation of β-klotho Liver specific knockout mice

C57BL/6J mice with the β-klotho gene floxed were generated by Shanghai Nanfang Center for Model Organisms. The targeting construct containing the two loxP sites flanking the exon 2 of the β-klotho gene and the FRT-flanked neomycin selection cassette (supplementary Fig.7A) was electroporated into embryonic stem cells, followed by selection of positive ES clones, microinjection and chimera identification as described previously[14].Chimeric males were mated withC57BL/6Jfemales for at least 8 generations to produce homologous β-klotho-floxed mice (β-klotho$^{f/f}$) in C57BL/6 background. Genotypes of mice were determined by PCR using the following primers: P1 (5'- TGTTGGGGCCATCTAAAATGG -3'), P2 (5'- GCCAAGACAAACATATTCGGG -3'), which produces a 216-bp fragment for the β-klotho-floxed locus, and a 132-bp fragment for wild-type (WT) locus respectively.

To generate β-klotho liver-specific knockout (Klb-LKO) mice**,** 1×10^{12} genomic particles of adeno-associated virus encoding Cre recombinase (AAV-Cre) or green fluorescent protein (AAV-GFP, as wild-type control) under the control of the mouse *apoE* gene promoter (which drives hepatocyte-specific gene expression) were intravenously injected into β-klotho$^{f/f}$ mice as previously reported[15]. After 4 weeks of AAV injection, mice were sacrificed to obtain various tissues for Western blot analysis to obtain liver-specific deletion of β-klotho.

References

1. Hotta Y, Nakamura H, Konishi M, Murata Y, Takagi H, Matsumura S, Inoue K, Fushiki T, Itoh N. Fibroblast growth factor 21 regulates lipolysis in white adipose tissue but is not required for ketogenesis and triglyceride clearance in liver. *Endocrinology*. 2009;150:4625-4633
2. Xu A, Wang Y, Keshaw H, Xu LY, Lam KS, Cooper GJ. The fat-derived hormone adiponectin

alleviates alcoholic and nonalcoholic fatty liver diseases in mice. *J Clin Invest*. 2003;112:91-100

3. Chen W, Hoo RL, Konishi M, Itoh N, Lee PC, Ye HY, Lam KS, Xu A. Growth hormone induces hepatic production of fibroblast growth factor 21 through a mechanism dependent on lipolysis in adipocytes. *J Biol Chem*. 2011;286:34559-34566
4. Lin Z, Tian H, Lam KS, Lin S, Hoo RC, Konishi M, Itoh N, Wang Y, Bornstein SR, Xu A, Li X. Adiponectin mediates the metabolic effects of fgf21 on glucose homeostasis and insulin sensitivity in mice. *Cell Metab*. 2013;17:779-789
5. Tangirala RK, Rubin EM, Palinski W. Quantitation of atherosclerosis in murine models: Correlation between lesions in the aortic origin and in the entire aorta, and differences in the extent of lesions between sexes in ldl receptor-deficient and apolipoprotein e-deficient mice. *J Lipid Res*. 1995;36:2320-2328
6. Paigen B, Morrow A, Holmes PA, Mitchell D, Williams RA. Quantitative assessment of atherosclerotic lesions in mice. *Atherosclerosis*. 1987;68:231-240
7. McGrath LT, Elliott RJ. Lipid analysis and fatty acid profiles of individual arterial atherosclerotic plaques. *Anal Biochem*. 1990;187:273-276
8. Turley SD, Herndon MW, Dietschy JM. Reevaluation and application of the dual-isotope plasma ratio method for the measurement of intestinal cholesterol absorption in the hamster. *J Lipid Res*. 1994;35:328-339
9. Li T, Matozel M, Boehme S, Kong B, Nilsson LM, Guo G, Ellis E, Chiang JY. Overexpression of cholesterol 7alpha-hydroxylase promotes hepatic bile acid synthesis and secretion and maintains cholesterol homeostasis. *Hepatology*. 2011;53:996-1006
10. Pfaffl MW. A new mathematical model for relative quantification in real-time rt-pcr. *Nucleic Acids Res*. 2001;29:e45
11. Xu A, Lam MC, Chan KW, Wang Y, Zhang J, Hoo RL, Xu JY, Chen B, Chow WS, Tso AW, Lam KS. Angiopoietin-like protein 4 decreases blood glucose and improves glucose tolerance but induces hyperlipidemia and hepatic steatosis in mice. *Proc Natl Acad Sci U S A*. 2005;102:6086-6091
12. Xu A, Suh PG, Marmy-Conus N, Pearson RB, Seok OY, Cocco L, Gilmour RS. Phosphorylation of nuclear phospholipase c beta1 by extracellular signal-regulated kinase mediates the mitogenic action of insulin-like growth factor i. *Mol Cell Biol*. 2001;21:2981-2990
13. Fruebis J, Tsao TS, Javorschi S, Ebbets-Reed D, Erickson MR, Yen FT, Bihain BE, Lodish HF. Proteolytic cleavage product of 30-kda adipocyte complement-related protein increases fatty acid oxidation in muscle and causes weight loss in mice. *Proc Natl Acad Sci U S A*. 2001;98:2005-2010
14. Cheng KK, Zhu W, Chen B, Wang Y, Wu D, Sweeney G, Wang B, Lam KS, Xu A. The adaptor protein appl2 inhibits insulin-stimulated glucose uptake by interacting with tbc1d1 in skeletal muscle. *Diabetes*. 2014;63:3748-3758
15. Li Z, Li Y, Chakraborty M, Fan Y, Bui HH, Peake DA, Kuo MS, Xiao X, Cao G, Jiang XC. Liver-specific deficiency of serine palmitoyltransferase subunit 2 decreases plasma sphingomyelin and increases apolipoprotein e levels. *J Biol Chem*. 2009;284:27010-27019

Supplementary Table1: A list of PCR primers used in this study.

Genes	Forward primer 5' to 3'	Reverse primer 5'to 3'
Mouse adiponectin	AGACCTGGCCACTTTCTCCTCATT	AGAGGAACAGGAGAGCTTGCAACA
Mouse CYP7A1	CTGTCATACCACAAAGTCTTATGTCA	ATGCTTCTGTGTCCAAATGCC
Mouse CYP8B1	GCAAGAAGATCCACCACTAC	ATCTCGCTGAGGGCAAAG
Mouse HMGCR	TCAGTGGGAACTATTGCACCGACA	TGGAATGACGGCTTCACAAACCAC
Mouse HMGCS	GATGAAAAGCACAGAAGAAC	CCTCACAGAGTATCTTAATG
Mouse SHP	CTATTCTGTATGCACTTCTGAGCCC	GGCAGTGGCTGTGAGATGC
Mouse ICAM-1	CCATCACCGTGTATTCGTTTC	AGGTCCTTGCCTACTTGCT
Mouse VCAM-1	TTGGGAGCCTCAACGGTACT	GCAATCGTTTTGTATTCAGGGGA
Mouse MCP-1	GCAGCAGGTGTCCCAAAGAA	ATTTACGGGTCAACTTCACATTCAA
Mouse TNF-α	TCCTTCAGACACCCTCAACC	GAGGCCCCAGTTTGAATTCTT
Mouse Faqs	GGAGGTCCTAGAGTACAATGCC	AAGCCTGGAGCAGTTCTACAC
Mouse Sqle	AGGAAGTTTTGGCCTCAGGA	AAACACACTCTGGTTCCGGA
Mouse Srebp-1	ACAGCGGTTTTGAACGACAT	CAGAGAGGAGGCCAGAGAAG
Mouse Srepb-2	AAGCTGGGCGATGGATGAG	ATCTCGTCGATGTCCCCG
Mouse LXRα	GAGTTGTGGAAGACAGAACCTCAA	GGGCATCCTGGCTTCCTC
Mouse FXR	CTGACGCCAGCGAATCTCA	CATCTTTTGCCTAGCCCATTCT
Mouse β-actin	GGCTGTATTCCCCTCCATCG	CCAGTTGGTAACAATGCCATGT

Supplementary Table 2: The oligonucleotides used for construction of adenoviral siRNA for Srebp-2, FGFR2, FGFR3, FGFR4 and scrambled control.

Name	Sequence of oligonucleotides
Sh-Srebp-2 *(forward)*	5'-CAC CGA AGA GTG GAT CTG TAC AAT AACGAA GAG GAA GGC CAT TGA TTA C -3'
Sh-Srebp-2*(reverse)*	5'-AAA AAA GAG TGG ATC TGT ACA ATA ATTCGGAG GAA GGC CAT TGA TTA C -3'
Sh-scramble *(forward)*	5'-CACCGAATATTATTAAGGCGACAGAGCGAACTCTGTCGCCTTAATAATATT-3'
Sh-scramble *(reverse)*	5'-AAAAAATATTATTAAGGCGACAGAGTTCGCTCTGTCGCCTTAATAATATTC-3'
Sh-FGFR4*(forward)*	5'-CAC CGAGCCGACACAAGAACAUCAUCGAAGAG GAA GGC CAT TGA TTA C -3'
Sh-FGFR4*(reverse)*	5'-AAA AAAAUGAUGUUCUUGUGUCGGCTTCGCTCTGTCGCCTTAATAATATTC -3'
Sh-Scramble *(forward)*	5'-CACCGAUUCUCCGAACGUGUCACGUCGAACTCTGTCGCCTTAATAATATT-3'
Sh-Scramble *(reverse)*	5'-AAAAAAACGUGACACGUUCGGAGAATTCGCTCTGTCGCCTTAATAATATTC-3'
Sh-FGFR2*(forward)*	5'-CAC CGAGGAGCACCGUACUGGACCA CGAACTCTGTCGCCTTAATAATATT-3'
Sh-FGFR2*(reverse)*	5'-AAAAAAAGGAGCACCGUACUGGACCA TTCGCTCTGTCGCCTTAATAATATTC-3'
Sh-Scramble *(forward)*	5'-CACCGAUUCUGCGATCAUGUCACGU CGAACTCTGTCGCCTTAATAATATT-3'
Sh-Scramble *(reverse)*	5'-AAAAAAACGUGACACGAUCAGAGAATTCGCTCTGTCGCCTTAATAATATTC-3'
Sh-FGFR3*(forward)*	5'-CAC CGA CGACAAGGAGCTAGAGGTT CGAACTCTGTCGCCTTAATAATATT-3'
Sh-FGFR3*(reverse)*	5'-AAAAAAA CGACAAGGAGCTAGAGGTTTTCGCTCTGTCGCCTTAATAATATTC-3'
Sh-Scramble *(forward)*	5'-CACCGATCTTAATCGCGTATAAGGCCGAACTCTGTCGCCTTAATAATATT-3'
Sh-Scramble *(reverse)*	5'-AAAAAAATCTTAATCGCGTATAAGGCTTCGCTCTGTCGCCTTAATAATATTC-3'

Supplemental Figures and Figure Legends

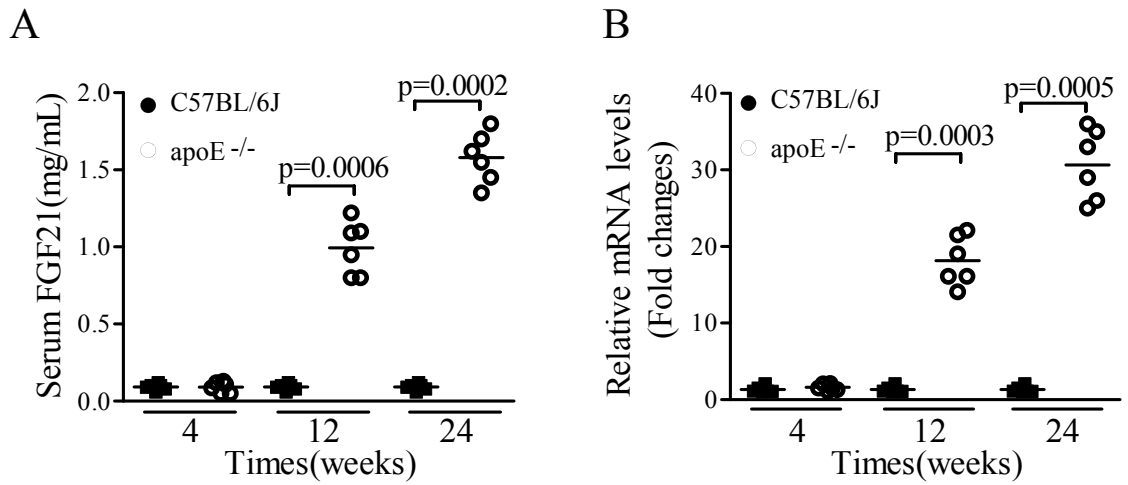

Supplemental Figure 1. Dynamic changes in circulating levels and hepatic mRNA expression of FGF21 in apoE$^{-/-}$ mice and C57BL/6J mice. The tissue samples were collected at 4-, 12- and 24-week-old male mice. (A**)** Serum levels of FGF21 measured with an immunoassay. (B) The mRNA expression level of FGF21 in the liver as determined by real-time PCR. n=6. Data are presented as dot plots with the line indicating the median. Statistical analysis was performed using repeated measure ANOVA.

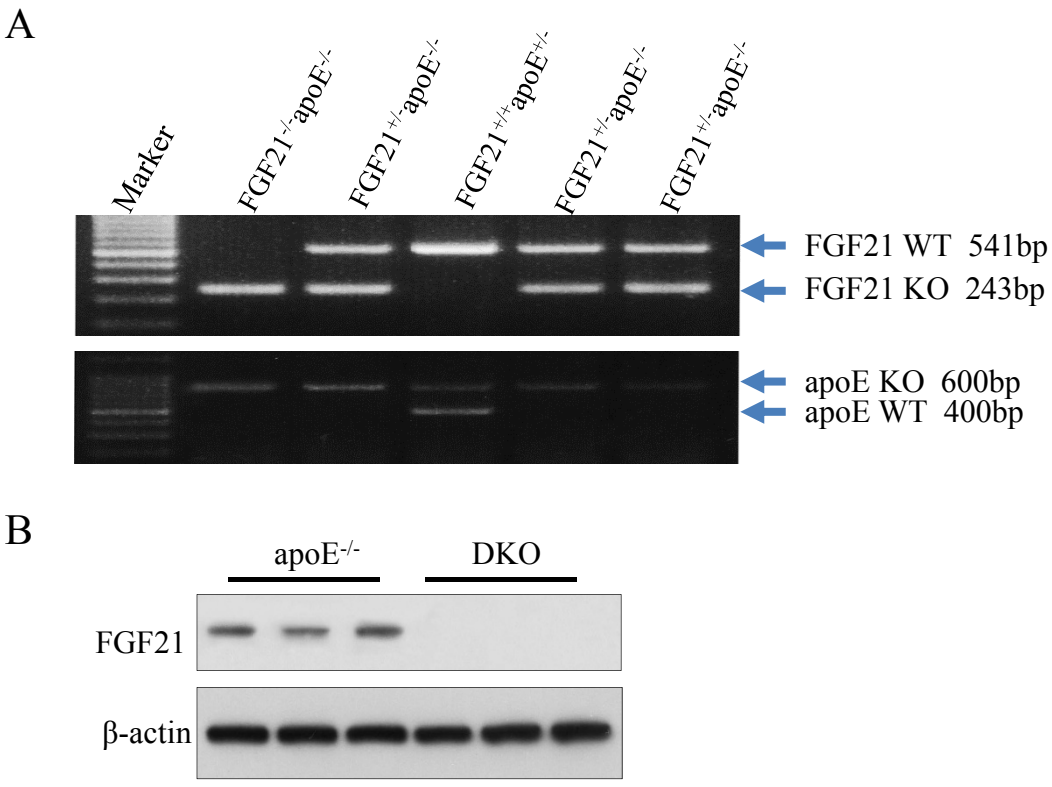

Supplemental Figure 2. Genotyping of FGF21$^{-/-}$apoE$^{-/-}$ (DKO) mice. FGF21 KO mice were generated by replacing most of exon 1 and all of exons 2 and 3 of the FGF21 gene with the IRES-LacZ-polyA/PGK-neo cassette. Genotypes of mice were determined by PCR using the following primers: P1-Fgf21 (5'-GACTGTTCAGTCAGGGATTG-3'), P2-Fgf21 (5'-CCCGTGATATTGCTGAAGAG-3'), and P3-Fgf21 (5'-ACAGGGTCTCAGGTTCAA AG-3'). P1 and P3 produced a 541-bp fragment of the wild-type (WT) *Fgf21* locus. P2 and P3 produced a 243-bp fragment of a mutant *Fgf21* locus. Genotypes of apoE$^{-/-}$ mice were determined by PCR using the following primers: P1-apoE (5'-TAT CTA AAC AGA CTC CACAGCCTCCAGACC-3'), P2-apoE (5'-GACTGGGCACA ACA GAC AAT CGG CTG CTCT-3'), P3-apoE (5'-CGAAGCCAGCTTGAGTTACAGAATG GGATC -3'). P1 and P3 produced a 400-bp fragment of the wild-type *apoE* locus. P2 and P3 produced a 600-bp fragment of a mutant *apoE* locus. (A) Representative PCR genotyping results. (B) Confirmation of FGF21 protein deficiency in the liver tissue of DKO mice by immunoblotting analysis.

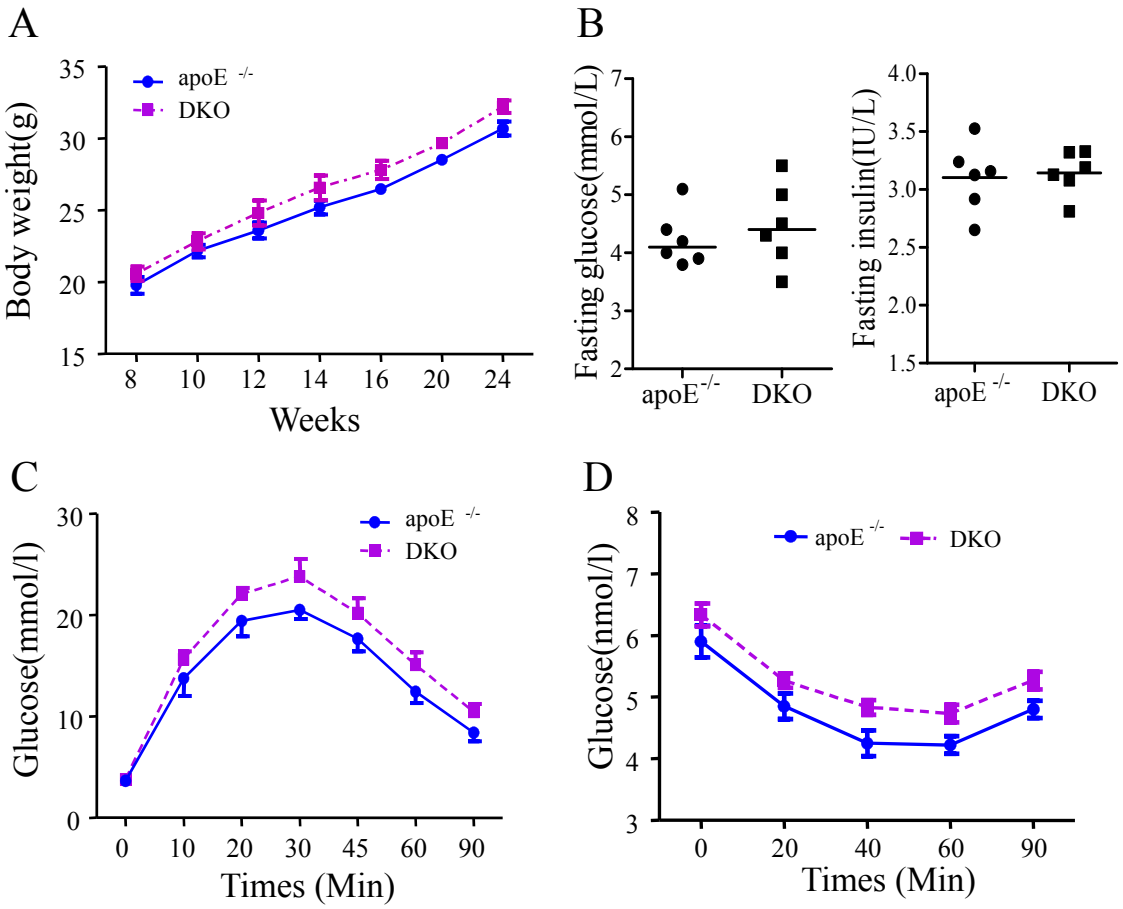

Supplemental Figure 3. FGF21 deficiency does not influence body weight, glucose tolerance and insulin sensitivity in apoE$^{-/-}$ mice. DKO and apoE$^{-/-}$ mice on standard chow were monitored for (A) body weight, (B) glucose and insulin levels, (C,D) Glucose and insulin tolerance tests were performed at 19 and 20 weeks after birth respectively. n=6. Data are presented as mean ± SEM（A, C and D) or dot plots with the line indicating the median（B）.

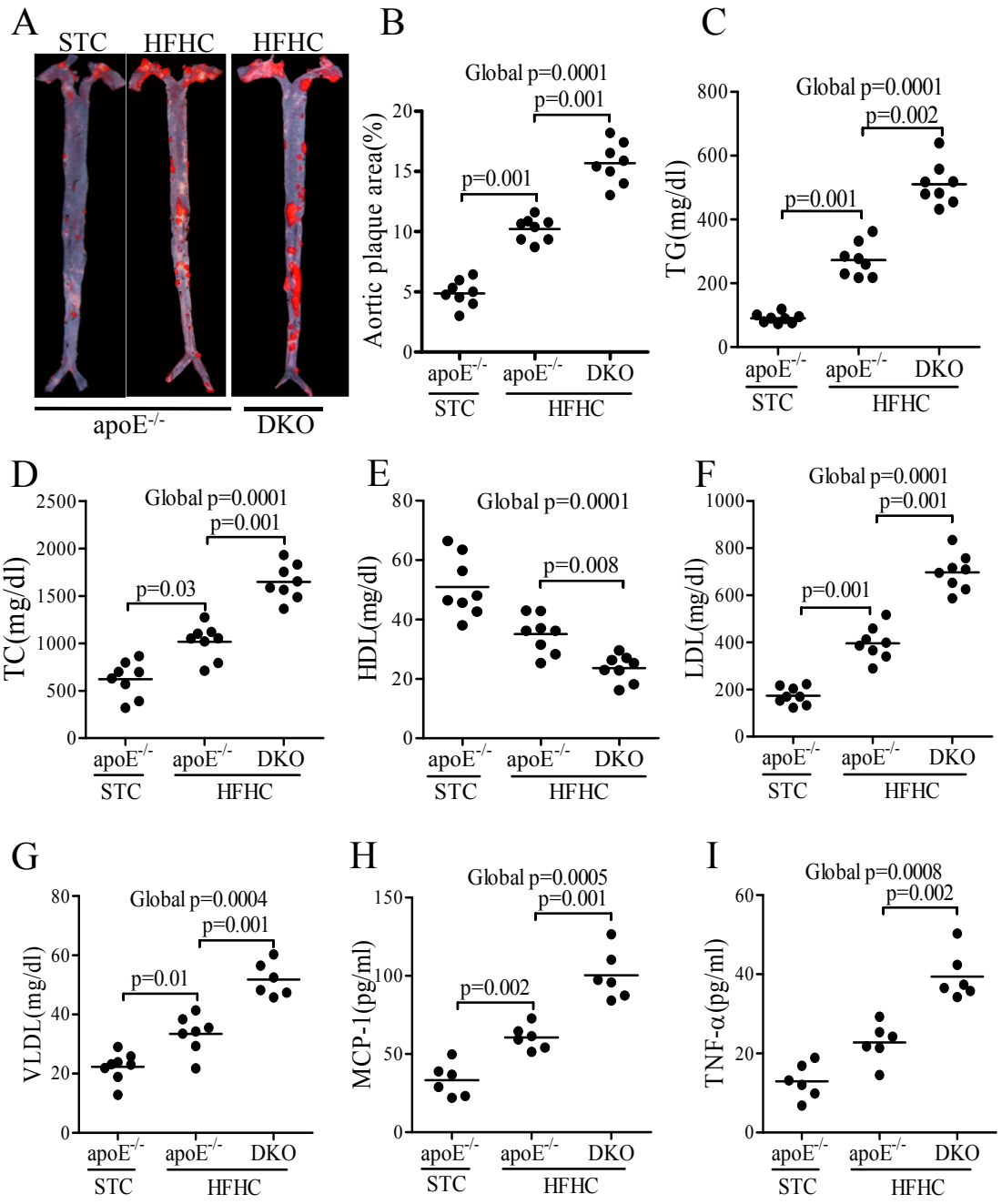

Supplemental Figure 4. FGF21 deficiency exacerbates HFHC diet-induced atherosclerosis, hyperlipidemia and inflammation. 8-week-old apoE$^{-/-}$ mice or DKO mice were fed with HFHC diet for a period of 12 weeks. STC-fed apoE$^{-/-}$ mice were included as a control. (A) *En face* staining of entire aortas with Oil red O. (B) Quantification of aortic plaque areas. (C-G) Serum lipid profiles, including triglycerides (TG), total cholesterol (TC), high density lipoprotein (HDL), low density lipoprotein (LDL) cholesterol, very low density lipoprotein (VLDL). (H,I) Serum levels of MCP-1 and TNF-α. n = 6-8. ***, $p<0.001$ *vs.* vehicle. Data are presented as dot plots with the line indicating the median. The global significance among three groups was determined by Kruskal-Wallis test, followed by pairwise comparisons with a Dunn-Sidak procedure.

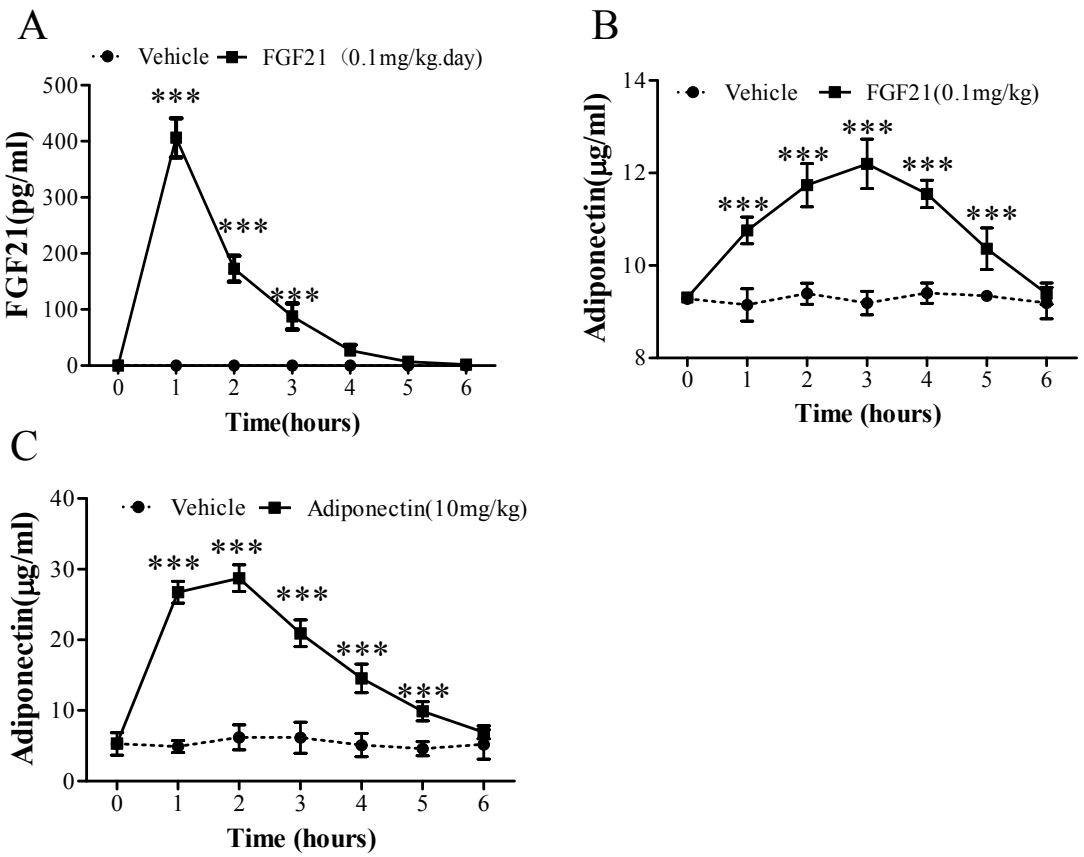

Supplemental Figure 5. Circulating levels of FGF21 and adiponectin in DKO mice after intraperitoneal administration of recombinant mouse FGF21 or adiponectin. Serum samples were collected every hour until 6 hours after DKO mice were intraperitoneally injected with FGF21 (0.1 mg/Kg.day), adiponectin (10 mg/Kg.day) or PBS as vehicle control. (A-B) Serum levels of FGF21 and adiponectin at different time points after injection with FGF21. (C) Changes in serum levels of adiponectin after administration with recombinant mouse adiponectin. Note that serum FGF21 is not detectable in DKO mice. n = 5. ***, $p<0.001$ *vs.* vehicle. Data are presented as mean ± SEM. Repeated measure ANOVA was used for comparison between two groups at each time points.

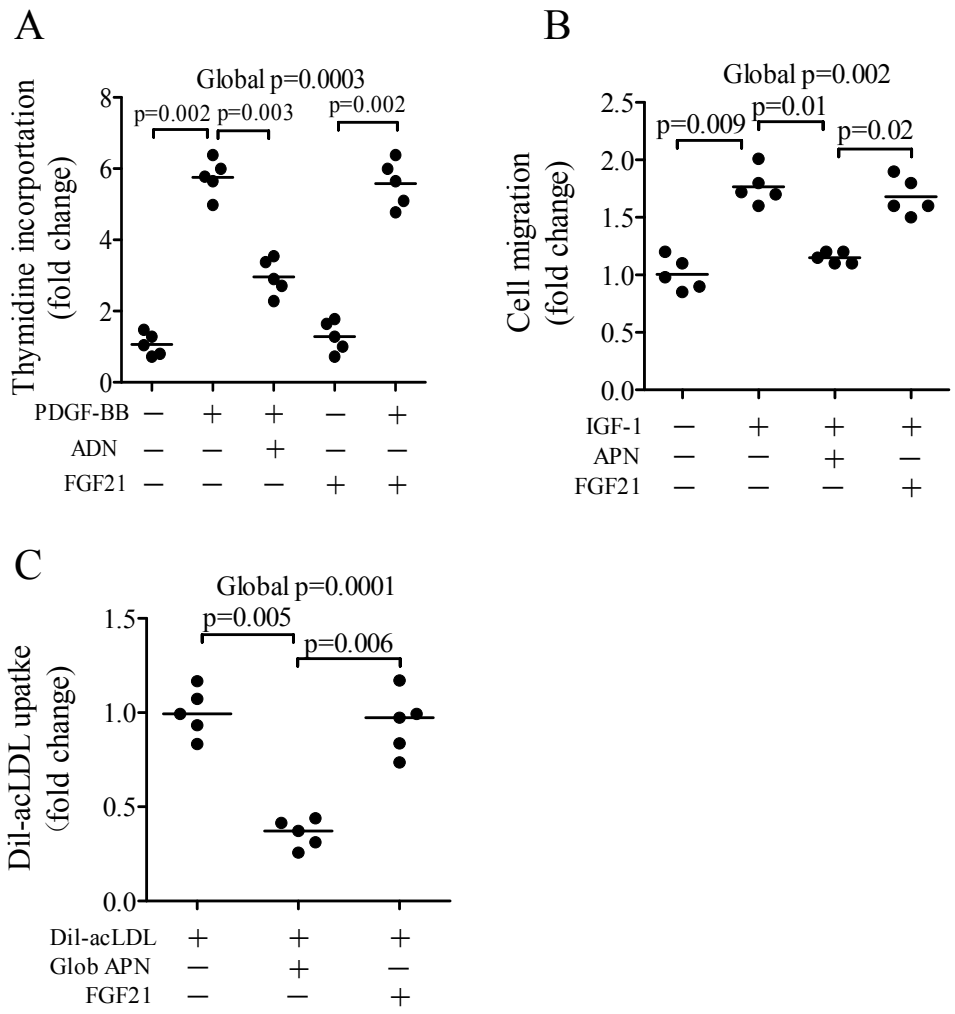

Supplemental Figure 6. Adiponectin，but not FGF21, directly suppresses smooth muscle cell proliferation and migration, and LDL uptake of macrophages. (A,B) Human aortic smooth muscle cells were treated with PDGF-AA (0.1μg/ml), adiponectin (ADN, 2.0μg/ml) or recombinant mouse FGF21 (50ng/ml) for 24 hours. The cell proliferation (A) and migration (B) was determined by ^{3}H-thymidine incorporation assay and a modified Boyden chamber assay described in respectively. (C) Primary mouse peritoneal macrophages were treated with ADN (2.0μg/ml), recombinant mouse FGF21 (50ng/ml) or vehicle (PBS) for 24 hours, loaded with Dil-AcLDL (10μg/ml). The uptake of Dil-AcLDL was determined by flow cytometry as described in the method, and expressed as fold changes over untreated cells. n = 5. Data are presented as dot plots with the line indicating the median. The global significance among three groups was determined by Kruskal-Wallis test, followed by pairwise comparisons with the Dunn-Sidak procedure.

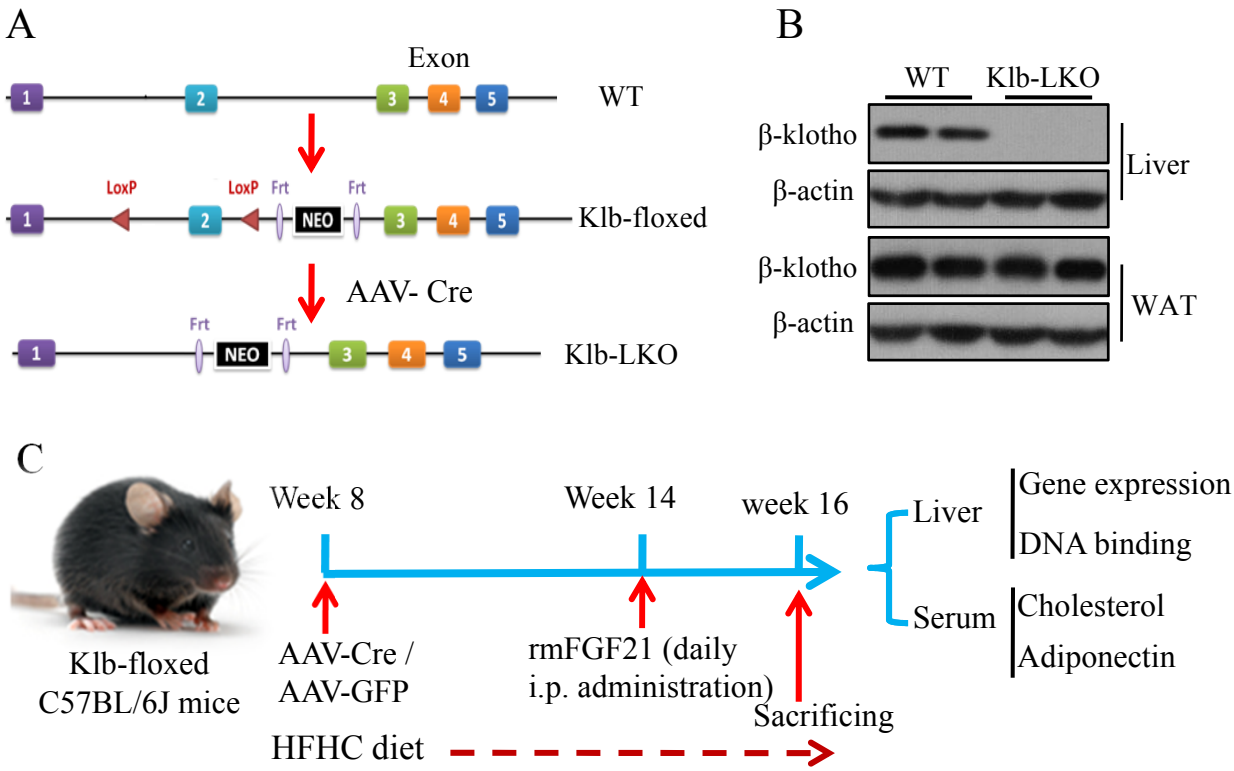
A
Exon
WT
LoxP
LoxP
Frt
Frt
NEO
Klb-floxed
AAV- Cre
Frt
Frt
NEO
Klb-LKO
B
WT
Klb-LKO
β-klotho
β-actin
Liver
β-klotho
β-actin
WAT
C
Klb-floxed
C57BL/6J mice
Week 8
Week 14
week 16
AAV-Cre /
AAV-GFP
rmFGF21 (daily
i.p. administration)
Sacrificing
HFHC diet
Liver
Gene expression
DNA binding
Serum
Cholesterol
Adiponectin
D
Srebp-2 mRNA levels
(fold change)
p=0.002
FGF21
WT
Klb-LKO
F
WT
WT+FGF21
Klb-LKO
Klb-LKO+FGF21
Relative mRNA levels
(fold change)
p=0.013
p=0.009
p=0.012
HMGCR
Fdps
HMGCS
E
DNA binding activity
(fold change)
p=0.001
FGF21
WT
Klb-LKO
G
Cholestrol(mg/dl)
p=0.001
FGF21
WT
Klb-LKO
H
Adiponectin(μg/ml)
NS
FGF21
WT
Klb-LKO

Supplemental Figure 7. The inhibitory effects of FGF21 on cholesterol biosynthesis are abrogated by liver-selective depletion of β-klotho. (A) Strategies for generating β-klotho liver-specific knockout mice (Klb-LKO) in C57BL/J background. 8-week-old β-klotho-floxed mice (Klb-floxed) were intravenously injected with 1×10^{12} genomic particles of adeno-associated virus encoding Cre recombinase (AAV-Cre) to delete the exon-2 region floxed with the two loxp sites for generation of β-klotho-LKO, or AAV encoding GFP as a wild-type (WT) controls. (B) Western blot analysis to confirm the specific deletion of β-klotho in the liver tissue in β-klotho-LKO mice, after 4 weeks of injection with AAV encoding Cre recombinase. Note that β-klotho remains unchanged in epididymal white adipose tissue (WAT) of Klb-LKO mice. The deletion of β-klotho can sustain for over 30 weeks after injection with AAV-Cre recombinase (data not shown). (C) A schematic diagram showing the study design for panel D-H. (D) The relative expression levels of Srepb-2 in the liver. (E) The DNA binding activities of Srebp-2 in the nuclear extracts of liver tissues. (F) The relative mRNA expression levels of genes involved in cholesterol synthesis including HMGCR, HMGCS and Fdps. (G) Serum total cholesterol levels. (H) Circulating levels of adiponectin. NS, not significant. n = 7. Data are presented as dot plots with the line indicating the median. Statistical analysis was performed with two-way ANOVA (D-H).

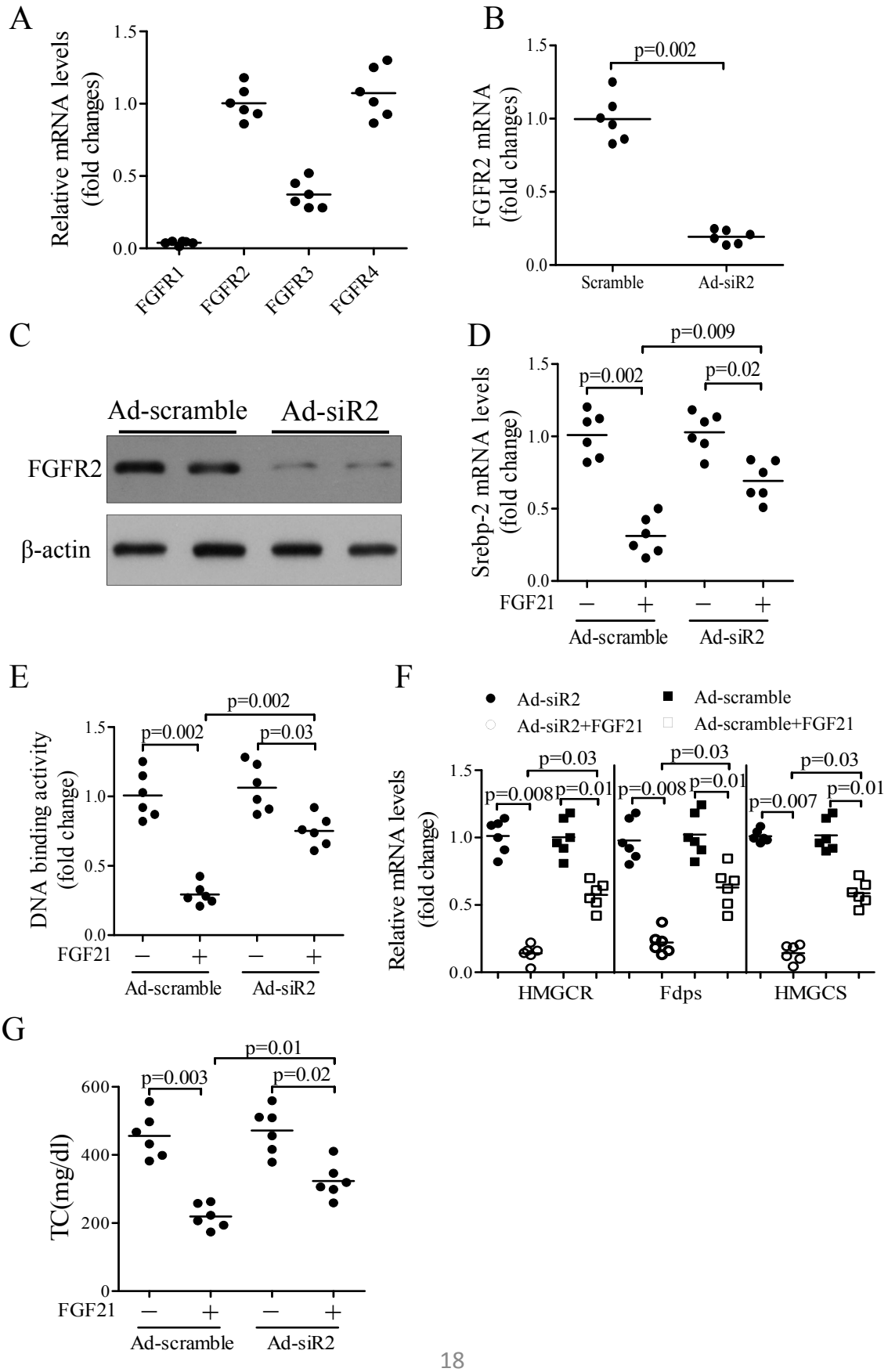
A
Relative mRNA levels (fold changes)
1.5
1.0
0.5
0.0
FGFR1
FGFR2
FGFR3
FGFR4
B
FGFR2 mRNA (fold changes)
p=0.002
Scramble
Ad-siR2
C
Ad-scramble
Ad-siR2
FGFR2
β-actin
D
Srebp-2 mRNA levels (fold change)
p=0.009
p=0.002
p=0.02
FGF21
Ad-scramble
Ad-siR2
E
DNA binding activity (fold change)
p=0.002
p=0.002
p=0.03
F
Ad-siR2
Ad-siR2+FGF21
Ad-scramble
Ad-scramble+FGF21
Relative mRNA levels (fold change)
p=0.03
p=0.008
p=0.01
HMGCR
Fdps
HMGCS
p=0.007
G
TC(mg/dl)
600
400
200
0
p=0.01
p=0.003
p=0.02

Supplemental Figure 8. Hepatic FGFR2 is involved in FGF21-mediated suppression of Srebp-2, expression of cholesterologenic genes and hypercholesterolemia. (A) The relative mRNA expression levels of the four FGFRs in the liver tissues of 12-week-old male C57BL/6J mice. (B-G) 10-week-old C57BL/6J mice on HFHC diet were intravenously injected with $1x10^9$ p.f.u of adenovirus encoding siRNA specific to FGFR2 (Ad-siR2) or scramble control (Ad-scramble) for 7 days, followed by daily intraperitoneal administration of rmFGF21 (0.1 mg/Kg) for another 7 days. (B, C) The relative mRNA and protein expression of FGFR2 in the liver at 14 days after the adenoviral administration. (D,E) The relative mRNA levels and DNA binding activities of Srebp-2 in the nuclear extracts of liver tissues. (F) The relative mRNA expression levels of genes involved in cholesterol synthesis including HMGCR, HMGCS and Fdps. (G) Serum total cholesterol (TC) levels. n = 6. Data are presented as dot plots with the line indicating the median. Statistical analysis was performed with Mann-Whitney U test (B) or two-way ANOVA (D-G) to compare two groups or multiple groups respectively.

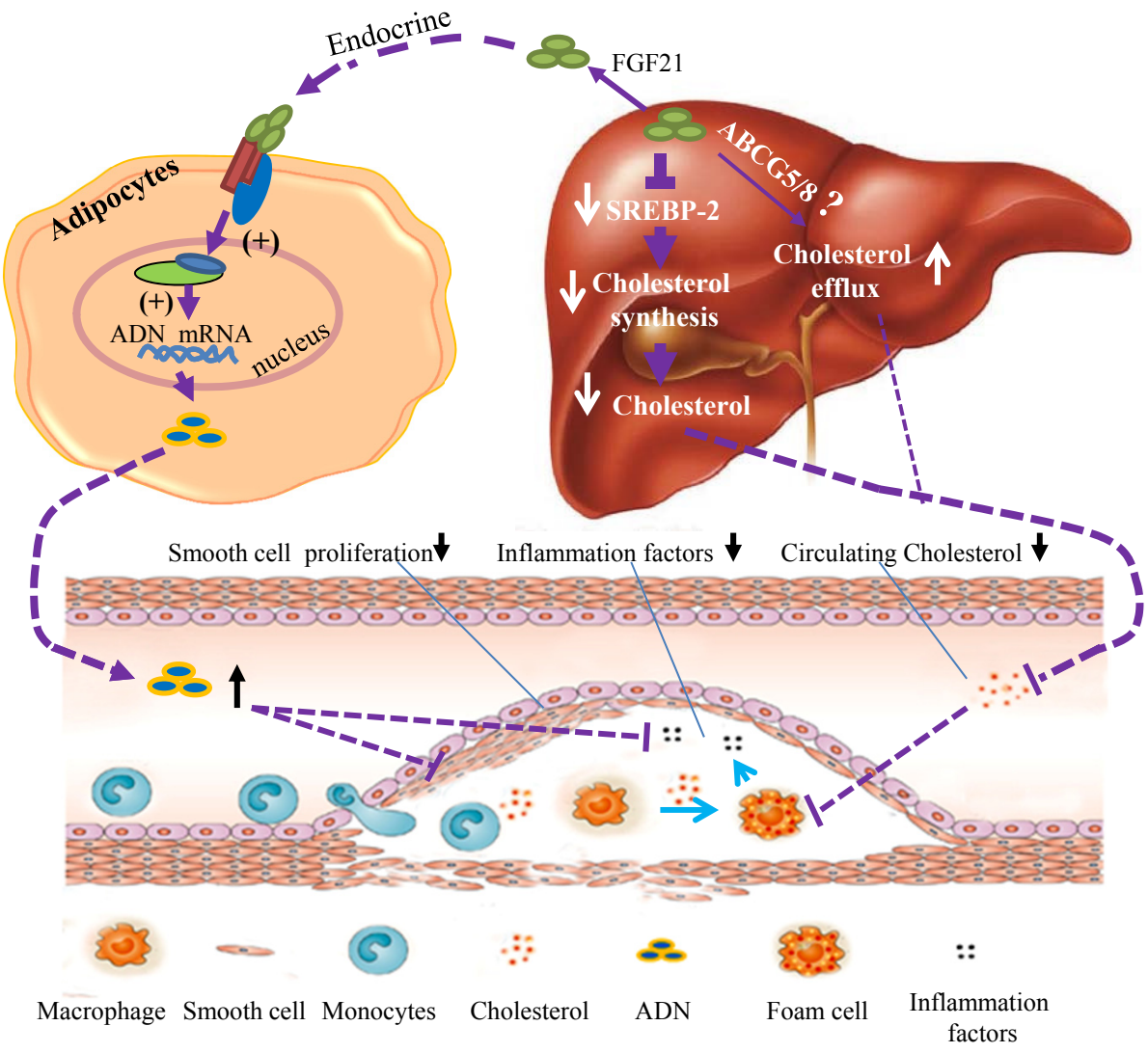

Supplemental Figure 9. The proposed mechanism whereby FGF21 suppresses atherosclerosis via induction of adiponectin (ADN) and suppression of Srebp-2.